Experimental Mechanics
https://doi.org/10.1007/s11340-026-01322-1

SP ISS: MECHANICS OF SOFT AND LIVING MATTER

# Time-Dependent Mechanics of Cellulose Nanofibril Gels Under Shear and Compression

S. Patel[1,2] · J. M. Considine[3] · J. Notbohm[1,2]

Received: 5 November 2025 / Accepted: 8 May 2026


## Abstract

**Background** Gels made of cellulose nanofibrils (CNF) are biodegradable and renewable with numerous applications. Prior efforts to quantify rheological properties have considered the material primarily as a fluid and have been hindered by strain localization and sample size dependence.

**Objective** We identify important considerations in designing experiments to quantify the time-dependent mechanics of CNF gels and devise experimental methods to quantify the viscoelastic properties of CNF gels on time scales on the order of hours.

**Methods** Shearing experiments were designed using a custom-built loading device to apply uniform shear strain while simultaneously imaging the sample for digital image correlation analysis, enabling quantification of the shear relaxation modulus. In parallel, triaxial experiments were performed by compressing thin CNF gels, enabling quantification of the creep compliance in response to changes in volume.

**Results** The shear data resulted in a relaxation modulus between 0.4 and 0.8 kPa at short times and a viscoelastic relaxation time on the order of tens of minutes. The triaxial compression tests revealed two regimes of strain response, which occurred above and below the osmotic pressure of the gels. Below the osmotic pressure, the creep compliance decreased with increasing compressive stress, whereas above the osmotic pressure, the creep compliance was relatively insensitive to the applied stress.

**Conclusions** Our study presents a summary of challenges in experiments on CNF gels and designs experimental methods that overcome limitations of prior work. The data quantifying relaxation modulus and creep compliance in response to changes in shape and volume complements data reported in prior literature. These methods and findings can be used in future studies to assess how composition and processing affects the viscoelastic properties of CNF gels.

**Keywords** Cellulose nanofibrils · Viscoelasticity · Digital image correlation · Osmotic pressure

## Introduction

Gels made of cellulose nanofibrils (CNF) are biodegradable and renewable, which make them appealing for use in several applications such as food packaging [1], 3D printing inks [2], and drilling fluids [2]. CNF hydrogels are comprised of water embedded with cellulose fibrils having widths of tens of nm and lengths of ∼1 μm. The material is often manufactured from wood pulp followed by chemical treatment and mechanical agitation. CNF gels are hydrophilic [3] and non-toxic [4]. Mechanical properties of dried CNF films have been quantified [5] as have properties of composites of CNF and epoxy [6] or CNF and polyacrylamide [7]. However, it remains a challenge to quantify the mechanical properties of CNF gels, which is in part due to their complex mechanics.

Much of the recent work to understand the mechanics of CNF gels has quantified the viscosity [8–22] and storage and loss moduli [7, 11, 12, 16, 17, 20, 23–27] across varying shear rates by using shear rheometers. However, the results have been inconsistent due to issues such as shear thinning

✉ J. Notbohm
jknotbohm@wisc.edu

1 Engineering Mechanics Program, University of Wisconsin–Madison, 1500 Engineering Dr, Madison, WI 53706, USA

2 Department of Mechanical Engineering, University of Wisconsin–Madison, 1500 Engineering Dr, Madison, WI 53706, USA

3 USDA Forest Service, Forest Products Laboratory, 1 Gifford Pinchot Dr, Madison, WI 53726, USA

Published online: 10 June 2026

[10, 11, 17, 19, 20, 23] and strain localization [17, 28], which cause the strain distribution to differ from assumptions made in calculating the shear viscosity or moduli from the experimental data. As a result, the results can depend on sample size [17], which means the properties measured by the rheometer are only effective properties, depending on both the sample geometry and the underlying material properties. Although some reports recognize this limitation [2, 10, 11, 14, 18, 19], there is no clear method for overcoming these issues with experiments using shear rheometers.

A second challenge is that CNF gels have typically been described as a fluid [11, 14, 20, 29, 30] which is a problematic perspective for two reasons. Firstly, many studies have reported the storage and loss moduli under sinusoidal loading and, from separate experiments, a shear viscosity as the material flowed [11, 12, 16, 17, 20]. These two sets of experiments are not directly comparable, because a nonzero storage modulus implies elastic storage of energy, which is missing in the second experiment reporting only a shear viscosity. It is unclear how to reconcile these observations into a consistent understanding of the mechanics. Secondly, viewing CNF gels from the perspective of a fluid leads to a focus on shape-changing (*i.e.*, shearing) flows. Still lacking is information on how the material responds to changes in volume.

Here we develop experimental methods to quantify the viscoelastic properties of CNF gels. Considering the challenges described above, the primary objectives are to account for strain localization under shear and, separately, to quantify the mechanics in response to changes in volume. Our study begins with a detailed summary of properties of CNF gels that must be considered when designing the experiments. We then implement two experimental approaches, studying the response of the material in shear and, separately, its response to triaxial compression, as follows. The first approach applied shear strain to CNF gels in a custom-built loading device. The applied deformation was held constant in time and digital image correlation (DIC) was used to account for heterogeneity and verify minimal localization in the strain field. The time-dependent force was quantified with a load cell over time periods of a few hours, enabling calculation of the shear relaxation modulus $G(t)$. The second approach applied compression to the top of a thin CNF gel. As a result of the small thickness, the boundary conditions created a nearly plane strain state, under which the material experienced a triaxial compressive stress state. The experiment was load-controlled and sample height was monitored over time, allowing for computation of a plane strain creep compliance $J(t)$. As the data will show, two regimes of strain response were apparent, which are described by a dependence on osmotic pressure.

## Methods

### Material Preparation

The CNF gels used in this work were prepared according to the process reported by Saito et al. [31]. Bleached eucalyptus pulp fibrils were carboxylated using 2,2,6,6-tetramethylpiperidine-1-oxyl (TEMPO), sodium bromide, and sodium hypochlorate as reactants at 25°C for 4 hr; the pH was maintained at pH 10 with sodium hydroxide. The oxidized pulp fibrils were then filtered and washed using deionized water. Carboxylate content was measured via titration based on TAPPI Test Method T237cm-98 and found to be 1.41 mmol/g COONa. The treated fibrils were diluted to 1.11 weight percent (wt%) suspension and passed four times through a homogenizer (GEA Niro Soavi, Model NS3015H, NH, USA) at 800-900 bar. Evaporating or adding water increases or decreases the concentration respectively. CNF gels above the given 1.11 wt% concentration were obtained by evaporating water from the gel via a hot plate at 100°C. To decrease the wt%, deionized water was vortex mixed with CNF gels. All gels were stored in a 4°C refrigerator to avoid mold and to minimize evaporation.

### CNF Properties and Considerations for Experimental Design

Before describing the experimental methods, we summarize in Fig. 1 properties of CNF gels that are important to consider. As described above, strain localization can occur under shear [17, 28] (Fig. 1(a)). In addition, gripping the material is challenging, and slip between the sample and grips is common [28] (Fig. 1(b)). CNF gels are nonlinear; many studies report shear thinning [8, 10–14, 16, 17, 19–23, 25, 32, 33] (Fig. 1(c)). Given that this material exhibits a nonzero storage modulus and is often described as being thixotropic [8, 10, 11, 13–15, 18, 30, 32], it is possible that it exhibits a yield stress (Fig. 1(d)).

Unless otherwise stated, all experiments were performed at 23.3°C ± 0.4°C (mean ± standard deviation across the different experiments). In preliminary experiments, we found that CNF gels exhibit elastocapillary behavior. In these experiments, DIC (as described in the next section) was used to quantify strains in CNF gels that were either circular (with radius ≈25.4 mm) or oval-shaped, elongated along the $x$ axis (with width of ≈25.4 mm and length of ≈76.2 mm). Note that only these preliminary experiments used circular and oval-shaped specimens. The gels were placed on glass coverslips, and individual $x$-$y$ planes through the glass coverslips were imaged on a spinning-disk confocal microscope (Yokogawa CSU-X1) with a 20× numerical aperture

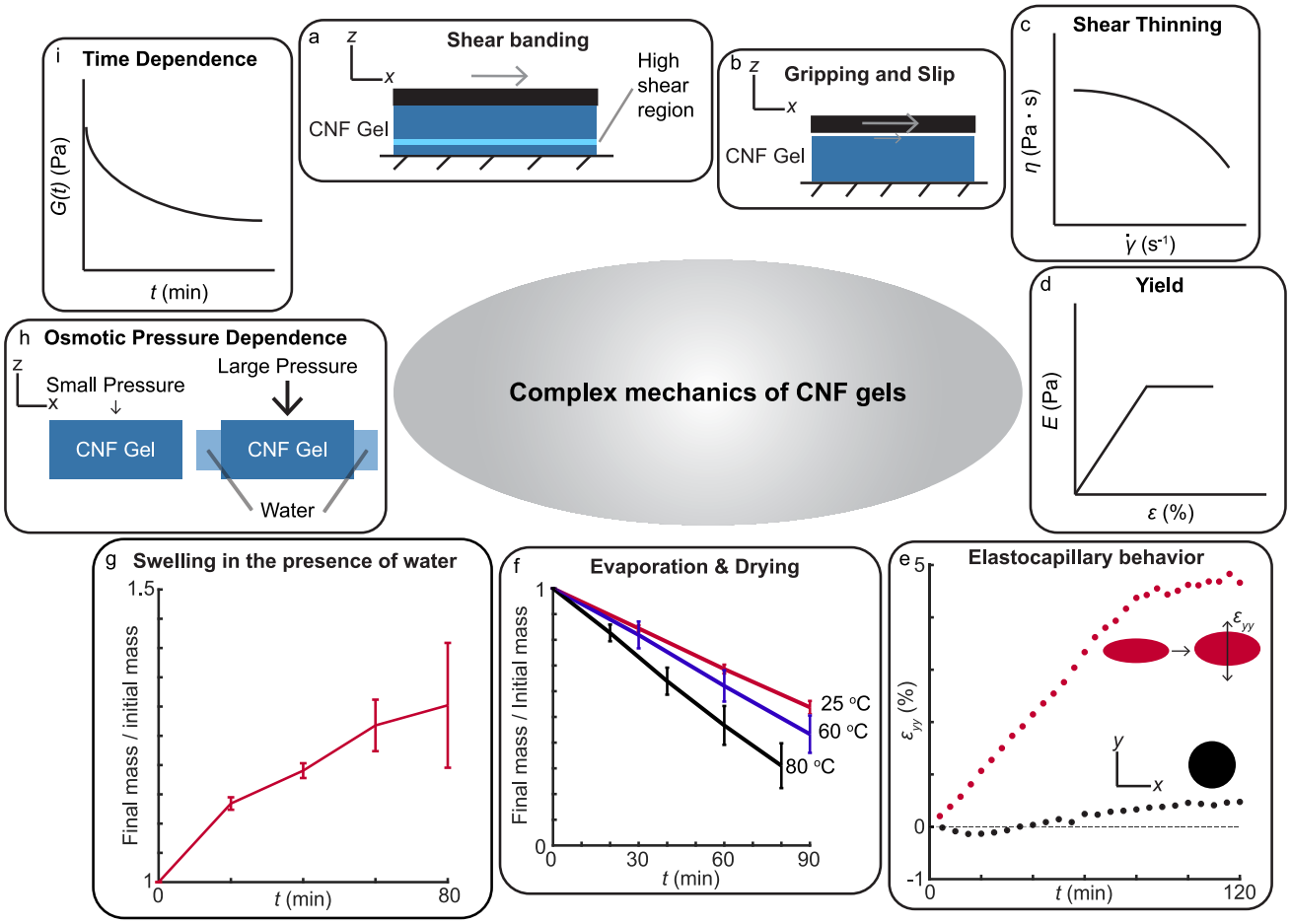


**Fig. 1** Summary of material properties and mechanical behaviors of CNF gels to account for in experimental design. (**a**) When subjected to shear strain, CNF gels can exhibit regions of high shear, called shear bands. (**b**) Gripping soft materials is often challenging, and reports have suggested there to be slip between grips and CNF gels, resulting in a difference between the applied displacement and gel deformation. (**c**) The apparent viscosity of CNF gels can decrease with shear rate, which is called shear thinning. (**d**) Experiments have reported both elastic modulus for small deformation and viscosity for large deformation, meaning there may exist a yield point after which the material flows. (**e**) Our preliminary experiments have indicated elastocapillary deformation in CNF gels. Samples were either circular (25.4 mm diameter) or elongated (76.2 mm × 25.4 mm). For the circular gels, strains were negligible, but for the elongated gels, $\varepsilon_{yy}$ was positive, indicating deformation that made the gels become more circular. (**f**) In environments of low relative humidity, water in CNF gels evaporates. Data shown are for 25.4 mm diameter samples at different temperatures. Lines indicate means and error bars are one standard deviation across 5 samples. (**g**) In the presence of water, CNF gels swell. Data shown are fractional change in mass of 25.4 mm diameter samples submerged in water. Line and error bars indicate mean and standard deviation across 4 samples. (**h**) As is shown later in the manuscript, CNF gels under pressure exhibit different behavior below and above a critical osmotic pressure. (**i**) Finally, the mechanics of CNF gels depend on time, as quantified in this manuscript

0.95 water-immersion objective (Nikon) and a Zyla camera (Andor). The normal strain in the $y$ direction, $\varepsilon_{yy}$, was nearly constant over time for the circular gels, but it increased over time for the oval-shaped gels (Fig. 1(e)). Because no force was applied to these gels and, as we show later, the shear modulus of this material is small, this deformation was driven by capillary effects that tend to make the elongated gel circular so as to minimize the ratio of perimeter to contact area between the gel and substrate.

We also quantified how quickly CNF gels of ≈25.4 mm diameter dried in a 40% relative humidity environment by measuring the mass at different time points, with results showing notable reductions in mass over time periods of tens of minutes (Fig. 1(f)). Sample evaporation cannot be prevented by submerging the sample in water, because CNF gels swell substantially when in direct contact with water. This is shown by swelling experiments that submerged CNF gels of ≈25.4 mm diameter in water and quantified the change in mass, which increased by tens of percent over time periods of tens of minutes (Fig. 1(g)).

As is shown in the Results section, our experiments demonstrate effects of an osmotic pressure, which, if exceeded, causes water to flow out of the material under volume-changing deformations (Fig. 1(h)). Finally, the goal of our study is to quantify time dependence, which we show visually by a hypothesized stress relaxation curve, and, as our

data will show, occurs over time periods of tens of minutes (Fig. 1(i)). The experimental approaches that we describe below will account for these numerous and complex material behaviors.

## Shear Experiments

A custom loading device was fabricated to produce simple shear. These experiments were performed in an enclosure that kept the environment at a relative humidity of 83% ± 4% and a temperature of 23.3°C ± 0.4°C. The relative humidity and temperature of the enclosure were monitored over time and varied by less than 1% and 1°C, respectively, during each experiment. A cartoon of the side view of the shearing device is shown in (Fig. 2(a)), and a simplified cartoon of the top view is shown in (Fig. 2(b)). The device used a fixed, rigid grip below the sample and a second rigid grip above the sample, both of which were 3D printed using PLA filament. Displacement of the upper grip was produced by a manual micrometer such that the strain rate was approximately 5% per second, with magnitude ranging from ∼0.1 to 1 mm, which produced shear strains ranging from 1 to 16%. A load cell (LSB200, FUTEK, 0.01-100 N) was mounted between the micrometer and upper grip to acquire force data from the deformed CNF gels, with a sampling frequency of 1 Hz. The load cell was calibrated with known masses before every experiment. The force data was low pass filtered using the "lowpass" function in Matlab, with a pass-band frequency one order of magnitude lower than the sampling frequency.

To improve gripping, the lower grip had a ribbed geometry spanning its entire length. Each rib was spaced approximately 1 mm apart and was approximately 0.5 mm tall.

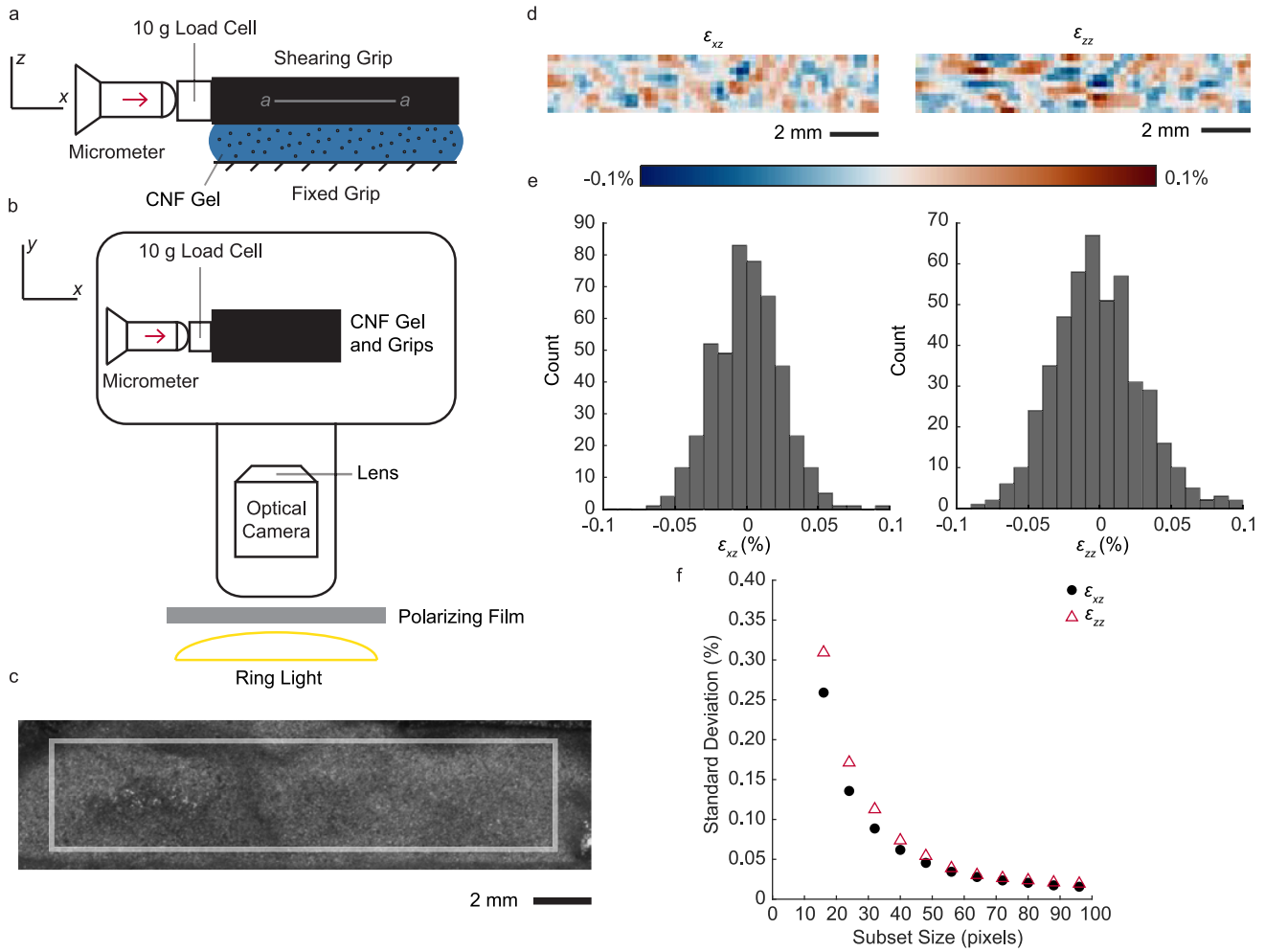


**Fig. 2** Schematic of shearing experiments and DIC noise floor. (**a, b**) Cartoon of the side view (a) and top view (b) of the shear experiment. The line denoting axis *a*-*a* defines the orientation of the upper shearing grip. (**c**) Representative image of a CNF gel speckled with iron powder, with the gray rectangle denoting the imaging region of interest. (**d**) Strain components $\varepsilon_{xz}$ and $\varepsilon_{zz}$ calculated from two undeformed images using a subset size of 64 × 64 pixels (≈ 1.07 × 1.07 mm). (**e**) Histograms of $\varepsilon_{xz}$ and $\varepsilon_{zz}$ calculated by DIC using a subset size of 64 × 64 pixels. The data approximately follow a normal distribution, and show that the noise does not exceed 0.1% strain. (**f**) Standard deviation of strain for varying subset sizes in the DIC algorithm

To improve gripping further, the upper grip had 2 mm long spikes arranged on a rectangular lattice and spaced approximately 4 mm apart that punctured the upper surface of the CNF gel. This grip was manually placed on the CNF gel, meaning it was not perfectly parallel throughout the experiment. The change in orientation of the upper grip was quantified by measuring the angle of axis *a*-*a* (Fig. 2(a)) of the upper grip over time. This angle changed by up to 1° over the duration of each experiment, which caused the shear strain to change by up to 1%. The weight of the upper grip was supported by the sample, producing a compressive normal stress of ≈50 Pa. Additionally, the stress due to the sample's own weight was ≈100 Pa. Our results in compression will show that this material exhibits an osmotic pressure that is an order of magnitude larger than these stresses. As such, little to no water can flow out of the samples due to these normal stresses. Additionally, capillary effects from adhesion to the upper grip prevented the CNF gel from spreading over the course of the experiment. Hence, although the normal stress through the thickness was nonzero during the shear experiments, it remained constant during each experiment, meaning effects on the shear relaxation modulus are expected to be negligible, and as will be shown later, the resulting strain field was still largely in a state of simple shear.

The prepared CNF gels had heights in the $z$-direction ranging from 4 to 8 mm. The gels had rectangular cross-sections, with lengths in the $x$-direction ranging from 14 to 22 mm and widths in the $y$-direction were 13 mm. The gels covered the entire contact between the upper and lower grip, meaning the contact area was constant over time, which prevented elastocapillary effects. The faces of the gels were speckled with iron powder (Alfa Aesar, 7439-89-6) using a 100 μm cell strainer. The iron powder was not mixed into the CNF gel, to avoid affecting the response of the sample in shear. Other materials for speckling were tested, and iron powder was found to produce the highest quality pattern for DIC analysis. The particle size of the iron powder was approximately 44 μm, which is small compared to the CNF gel dimensions described above. A representative image of a CNF gel speckled with iron powder is shown in (Fig. 2(c)). Visual analysis showed an average pattern feature size of approximately 5 × 5 pixels.

All images of the speckled CNF gels were taken with an Alvium Allied Vision optical monochrome camera (1800 U-511m, 5.1 megapixel) with an exposure time of 0.75 s and a Techspec UC Series lens (12 mm focal length, 70.3 mm field of view, 160 mm SOD). The Vimba-X image acquisition software (Alvium) was used during imaging. Each experiment lasted for 3 hr, with images being taken every 30 min after deforming the CNF gels. To improve image quality, the faces of the gels that were imaged were first flattened with a plastic spatula before speckling, which slightly reduced variability in the measured strain. A ring light was used to illuminate the speckled gel face, with a polarizing film sheet in between it and the camera to avoid reflections from the gel. Adding Kimwipes around the enclosure and in front of the polarizing film helped diffuse the light. All images were imported into ImageJ and Matlab for post-processing.

To avoid potential errors caused by strain localization in these experiments, the displacement and strain fields were quantified using two-dimensional DIC, using the Fast Iterative DIC algorithm [34] to compare each image in the deformed state to the undeformed configuration. The Fast Iterative DIC algorithm uses a first order shape function to quantify displacements. Strain fields were computed from the displacement gradient, which was calculated by convolution with a 5 × 5 kernel [35].

The DIC noise floor was quantified by computing strains on an unloaded CNF gel. In each experiment, two consecutive images of the CNF gel speckled with iron powder were taken. Representative strains $\varepsilon_{zz}$ and $\varepsilon_{xz}$, which were computed from the displacement field from DIC using 64 × 64 pixels ($\approx 1.07 \times 1.07$ mm$^2$) subsets, are shown in (Fig. 2(d)). Histograms of the quantified strains using a subset size of 64 × 64 pixels are shown in (Fig. 2(e)). For this subset size, the maximum magnitude of shear and normal strains were both approximately 0.1%, and the standard deviations were 0.03% strain. The standard deviation of strain was also computed for many subset sizes, which decreased with increasing subset size (Fig. 2(f)). The noise floor was computed for every experiment, and the data shown in (Fig. 2(d–f)) is representative of the results from multiple experiments. A subset size of 64 × 64 pixels ($\approx 1.07 \times 1.07$ mm$^2$) and spacing of 16 pixels ($\approx 0.27$ mm) was chosen for all experiments. The corresponding level of noise, ∼0.1% strain, is acceptable as the smallest magnitude of strain applied in the experiments was ∼2%. Strain data was acquired for the middle 80% of the field of view in each image. Strain data corresponding to the top or bottom 10% of the field of view was discarded.

## Triaxial Compression Experiments

The objective of our second experimental approach was to study the time-dependent response of the material to changes in volume. Producing a change in only volume, with no change in shape, is not feasible for this material given the water inside it. Hence, we adapted a recently published approach, which uses a thin sample and compresses it between rigid parallel plates [36–38]. A sketch of the experiment is shown in (Fig. 3(a)). The plate beneath the CNF sample was rigid and fixed. The upper plate was moved downward in the $z$ direction, compressing the sample. Assuming the presence of friction between the sample and plates, the displacements in the $x$ and $y$ directions can be assumed to be zero, which in turn means that the strains $\varepsilon_{xx}$ and $\varepsilon_{yy}$ are approximately zero. Therefore, this experiment produced an

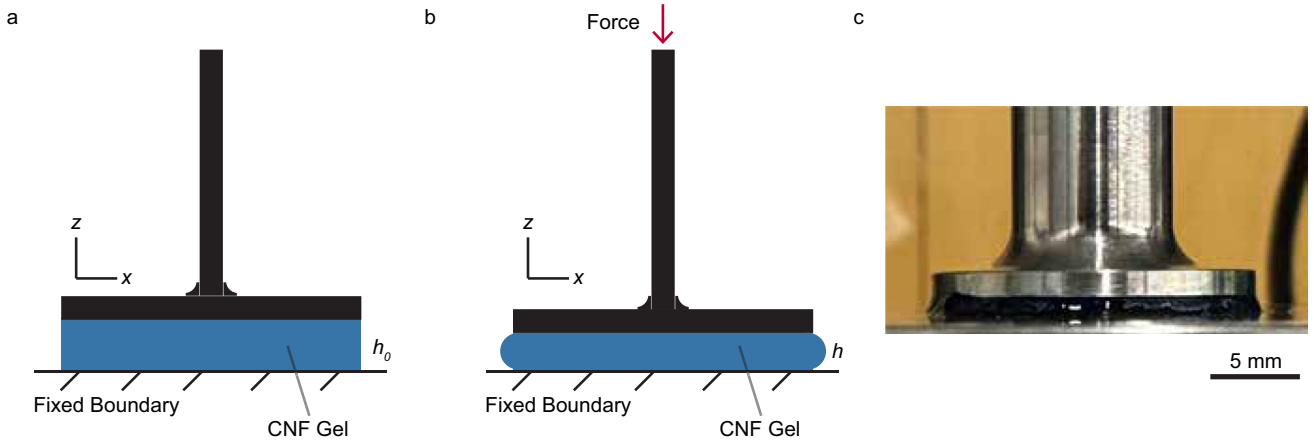


**Fig. 3** Schematic of triaxial compression experiments on CNF gels. (**a**) Cartoon of a CNF gel of initial height $h_0$ under no loading. (**b**) Cartoon of the CNF gel subjected to a compressive force. There is slight bulging at the sides, and the height of the gel during the experiment is denoted as $h$. (**c**) Representative image of a CNF gel mixed with food coloring under a compressive stress, showing bulging at the sides

approximately plane strain condition, except at the edges of the sample, where the sample can potentially bulge outwards (Fig. 3(b)). By St. Venant's Principle, errors caused by these edge effects are confined to a region of size approximately equal to the sample height $h = 1$ mm, and the errors will have negligible impact on the results if the sample diameter is large compared to the height. In these experiments, the diameter was 18 mm, meaning that by St. Venant's Principle, the central $\approx$16 mm of each sample was unaffected by the boundaries. To verify that the friction between the samples and grips were adequate to prevent slip, an image of a sample was captured, showing bulging at the sides and no bulging at the top or bottom (Fig. 3(c)), which verifies the that the sample was under an approximate state of plane strain.

If the sample were isotropic, linear, and elastic, the normal stresses in the $x$ and $y$ directions would be equal and related to the normal stress in the $z$ direction according to $\sigma_{xx} = \sigma_{yy} = \sigma_{zz}[\nu/(1-\nu)]$, where $\nu$ is Poisson's ratio. For an incompressible material ($\nu = 0.5$), $\sigma_{xx} = \sigma_{yy} = \sigma_{zz}$, and this experiment produces a state of hydrostatic pressure. As the data will show, the CNF gels used here have finite compressibility (*i.e.*, $\nu < 0.5$), for which $|\sigma_{xx}| = |\sigma_{yy}| < |\sigma_{zz}|$, meaning the stress state in the experiments will not be hydrostatic pressure but will nevertheless be a state of triaxial compression. Finally, because the boundaries along the circumference of the sample are traction free, the stress state is altered near the boundaries, but St. Venant's Principle again suggests that errors would be negligible for samples with large diameter compared to height.

The device used in this experiment was a rheometer (Kinexus Ultra+, Malvern), with a parallel circular plate geometry of diameter 18 mm. Samples were approximately 1 mm in height; the large aspect ratio (18:1) ensured triaxial compression as described above, and also slowed the rate of evaporation. The large aspect ratio also means that effects of the boundary on the stress state, as described above, will be negligible. The circular shape of the sample also prevented elastocapillary effects during the experiment. CNF gels were placed between the rheometer plates, and allowed to rest for a few minutes before beginning each experiment. A constant compressive force was applied for up to 1 hr, and the sample height was measured over time. This experiment was a load-control experiment, because the boundary conditions cause a change in both shape and volume. For a hypothetical sample that is thin and in the incompressible limit, the volume change is constrained to zero, meaning it would be fully rigid under this loading. Use of displacement control under these conditions would cause a very large force that could damage the load cell in the rheometer.

The engineering stress $\sigma_{zz}$ was computed by dividing the force by the sample area, and the engineering strain was computed from the sample height at each time point. This procedure was repeated for a range of applied stress from as small as 11 Pa to as large as 15 kPa, depending on the wt% of CNF in the sample. A different CNF sample was used for each applied compressive force. The experimental procedure was repeated for samples with CNF concentrations ranging from 0.95 to 5.0 wt%.

## Results and Discussion

### Shear Strain, Heterogeneous Strains, and Sample Size Independence

In response to shear, CNF gels undergo strain localization and shear banding [17, 28], which prevents use of standard equipment such as rheometers. To overcome this challenge, we applied shear to CNF while quantifying the strains by DIC. Images of shear strain $\varepsilon_{xz}$ for different samples are

shown in (Fig. 4(a–b)). The results showed that $\varepsilon_{xz}$ varied over space, with fluctuations sometimes equal to about half of the maximum strain in the field of view. These fluctuations were unlikely to be the result of noise, because the noise floor was much smaller (∼0.1% strain, Fig. 2(d–e)) and the spatial sizes of the regions of smaller and larger strain in (Fig. 4(a–b)) were visually larger than those in the noise floor experiment (Fig. 2(d)).

To determine whether the fluctuations in strain caused slip between the grips and samples, we quantified the spatial distribution of strain, focusing on the distribution through the height (*i.e.*, through the $z$ direction). To this end, we computed a mean of DIC-measured shear strain across the $x$ direction for each sample to obtain curves against $z$ position. Data were plotted by normalizing the mean shear strain against the maximum value of each data set (Fig. 4(c)). The maximal value of mean shear strain frequently did not occur near the bottom or top of the sample, indicating little apparent slip at the grips. Next, we computed a mean of the DIC-measured shear strain over all space, $\bar{\varepsilon}_{xz}$. (Hereafter, we use the overbar to indicate a mean over space.) For the different CNF samples, $\bar{\varepsilon}_{xz}$ was plotted against the applied strain, defined as $\varepsilon_{xz}^{\text{app}} = \delta/(2h)$, with $\delta$ being the displacement applied by the micrometer (Fig. 4(d)). (The factor of $1/2$ is used to be consistent with our definition of shear strain, which is $\varepsilon_{xz} = (\partial u/\partial z + \partial w/\partial x)/2$, with $u$ and $w$ being the displacements in the $x$ and $z$ directions.) The data were linearly proportional, and a linear regression gave a slope with a 95% confidence interval of $0.97 \pm 0.31$ ($R^2 = 0.83$), which is close to unity. Hence, the strain experienced by the material was close to the strain applied by the shearing device, indicating little apparent slip at the grips and no systematic shear banding in these experiments.

As a result of strain localization, prior reports have shown that the apparent modulus of CNF depends on sample thickness [17, 28]. If our experimental approach has effectively resolved the effects of strain localization, then the results should not depend on sample height. Therefore, we performed stress relaxation experiments for samples having a range of heights, varying from 3.63 to 7.75 mm. Approximately 9-10% $\varepsilon_{xz}^{\text{app}}$ was applied to all samples. Because we applied and held a fixed displacement on the top surface of the gel, if the gripping was effective, there would be a minimal change in the mean shear strain $\bar{\varepsilon}_{xz}$ over time. The shear strain was averaged over space for each sample and each time point. The results showed that $\bar{\varepsilon}_{xz}$ changed by no more than 1% over the duration of the experiment (Fig. 5(a)), which was caused by rotation of the upper grip, as described in the Methods section. We also quantified the spatial mean of the normal strain in the $z$ direction, $\bar{\varepsilon}_{zz}$, at each time point for each sample, which decreased by a couple percent for each gel over the course of 3 hr (Fig. 5(b)). This change in $\bar{\varepsilon}_{zz}$ is likely due to evaporation of water, as the relative humidity was not 100%.

Next, the shear relaxation modulus $G(t)$ was quantified by dividing the time-dependent shear stress $\sigma_{xz}(t)$ by the mean shear strain $\bar{\varepsilon}_{xz}$. As $\bar{\varepsilon}_{xz}$ was not exactly constant with time, the relaxation modulus $G(t)$ can only be an approximation, but since $\bar{\varepsilon}_{xz}$ varied by no more than 1% in time, errors in $G(t)$ are expected to be on the order of a few Pa. For the computation, we chose to use the DIC-measured value of $\bar{\varepsilon}_{xz}$ at each time point, rather than the initial value of $\bar{\varepsilon}_{xz}$. Given that

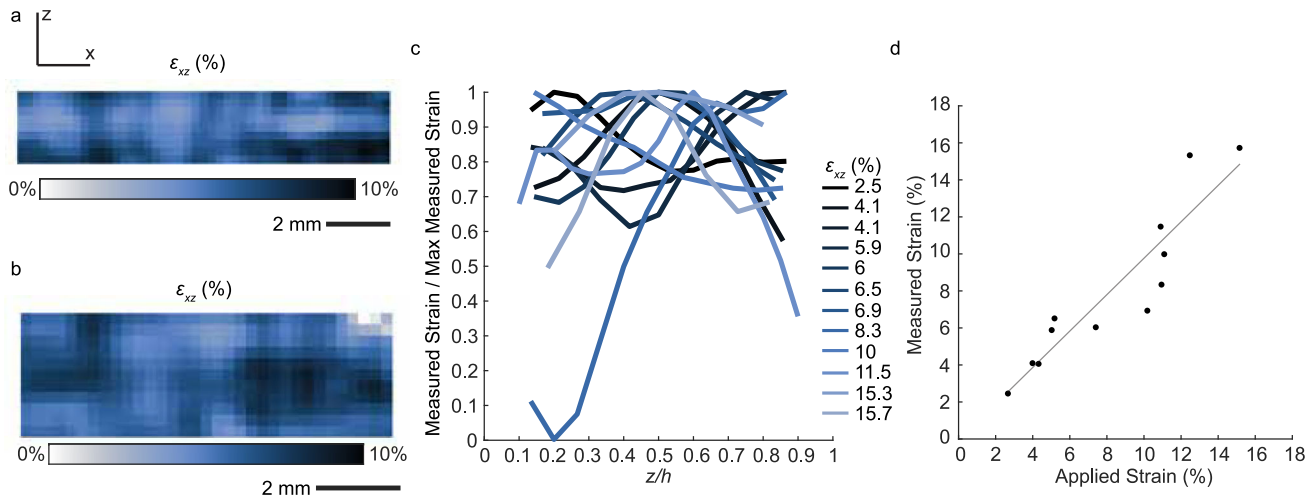


**Fig. 4** Spatial variability of strain in sheared CNF gels. (**a**–**b**) Shear strain fields in two representative CNF gels. The spatial variability in strain appears to be independent of sample height. (**c**) Shear strain normalized by maximum shear strain plotted against distance from the upper grip normalized by sample height shows no correlation, indicating no systematic shear banding and little apparent slip at the grips. (**d**) Shear strain in the gel quantified from DIC and averaged over space plotted against shear strain calculated from the displacement of the micrometer. The linear fit has a slope of 0.97 (with a 95% confidence interval 0.31), which is near unity, indicating minimal slip at the grips

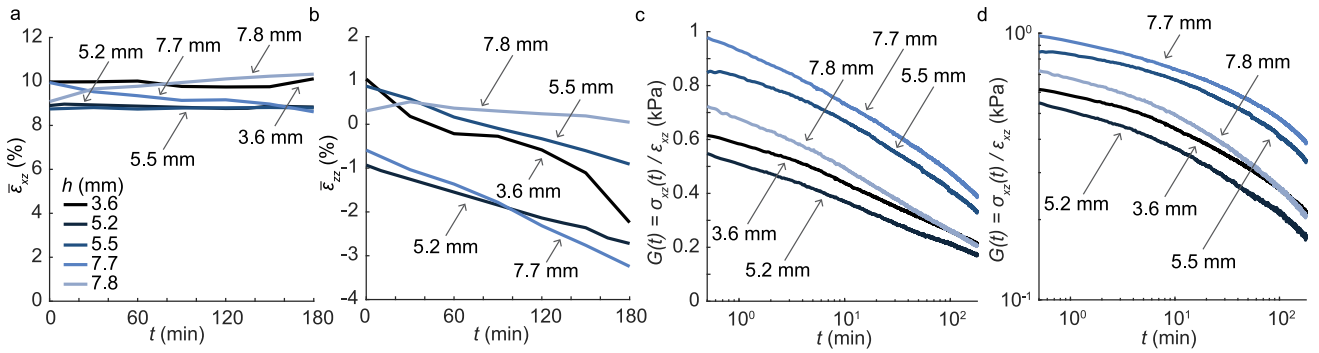


**Fig. 5** Confirming sample size independence in CNF gels subjected to shear strain with the custom loading device. (**a**) Mean shear strains in all CNF gels changed by no more than 1% over 3 hr. (**b**) Mean normal strain in the $z$-direction decreased by no more than 3% strain over 3 hr. (**c-d**) Relaxation modulus $G(t)$ plotted against time on (c) semi-log axes and (d) log-log axes

the temporal resolution of the shear stress data was higher than that of the DIC-measured shear strain, values of the mean shear strain $\bar{\varepsilon}_{xz}$ were interpolated between measured time points. Figure 5(c) and (d) display the relaxation modulus against time on semi-logarithmic and logarithmic axes, respectively. The data varied between the different samples, causing $G(t)$ to range by around 0.5 kPa. However, there was no clear relationship between relaxation modulus and sample height, which was confirmed by a Pearson's correlation test between sample height and relaxation modulus $G(t)$ at the 1 hr time point ($R = 0.11$, $p = 0.74$). As a result, it is unlikely that our experimental results depended on sample height, which is consistent with the results from Fig. 4, showing little apparent slip at the grips. Instead, the variability of the observed $G(t)$ likely comes from differences in the initial microstructure of each sample after sample preparation, such as fibril length, density, and orientation.

## Relaxation Modulus at Varying Shear Strain

Next, to test for potential nonlinearity, we subjected CNF gels to varying magnitudes of shear strain and quantified the relaxation modulus using the procedure described above. Each experiment was performed on a different sample. As above, the spatially averaged value of shear strain $\bar{\varepsilon}_{xz}$ was nearly constant in time (Fig. 6(a)), and did not change by more than 1% throughout any experiment. The spatially averaged normal strain $\bar{\varepsilon}_{zz}$ changed only slightly over time by no more than 4% for all samples (Fig. 6(b)). The value of $\bar{\varepsilon}_{zz}$ was uncorrelated to the applied shear strain $\bar{\varepsilon}_{xz}$, indicating that the nonzero values of $\bar{\varepsilon}_{zz}$ were unlikely to be caused by material behavior that couples shear and normal strains, as can occur in nonlinear materials [39].

The relaxation moduli $G(t)$ of the CNF gels subjected to the varying magnitudes of shear strain are shown in (Fig. 6(c) and (d)). The shear relaxation moduli ranged from 0.4–0.8 kPa at short time scales and were on the order of 0.1 kPa at long times. While this magnitude seems small, gels of biological fibrils such as collagen, fibrin, and vimentin at similar fibril concentration have shear moduli in the range of 0.01–0.1 kPa [40–42]. As above, there was notable variability in $G(t)$, by about a factor of two, between different samples. The data were not monotonic with applied shear strain. To study this observation more closely, we computed the shear stress at the $t = 1$ hr time point and plotted against strain for each sample. The data were approximately linear, albeit with some variability (Fig. 6(e)). These data indicate that for the range of strains applied here ($\approx$ 2–16%), the material behavior was approximately linear. While some literature reports that CNF gels of similar weight percent transition to a fluid when subjected to shear strains at or above 10% [15, 23], our data did not show a distinctly different behavior in relaxation modulus above this strain magnitude.

## Effects of Pre-Conditioning on Relaxation Modulus

The data reported in Fig. 6 showed large sample-to-sample variation. Those experiments did not pre-condition the samples. Some prior studies of CNF gels have incorporated pre-conditioning by ignoring the first few cycles of oscillatory loading or by pre-shearing the sample [8, 10, 13, 14, 17, 20, 30]. To determine if pre-conditioning reduces sample-to-sample variability, we added a pre-conditioning step to our experimental procedure. After CNF gels were placed between the grips, we applied and removed a displacement at the upper grip, and immediately applied the same magnitude of displacement again. The shear strain and relaxation moduli were quantified during the second loading. The results from these pre-conditioned CNF gels are shown in (Fig. 7(b)). The relaxation moduli $G(t)$ showed some variability, varying by tens of percent (Fig. 7(b)) compared to nearly 100% variability in the experiments without pre-conditioning in the same range of shear strains (Fig. 7(a)). We repeated the experiment again, adding a 1 hr wait time after the pre-conditioning step

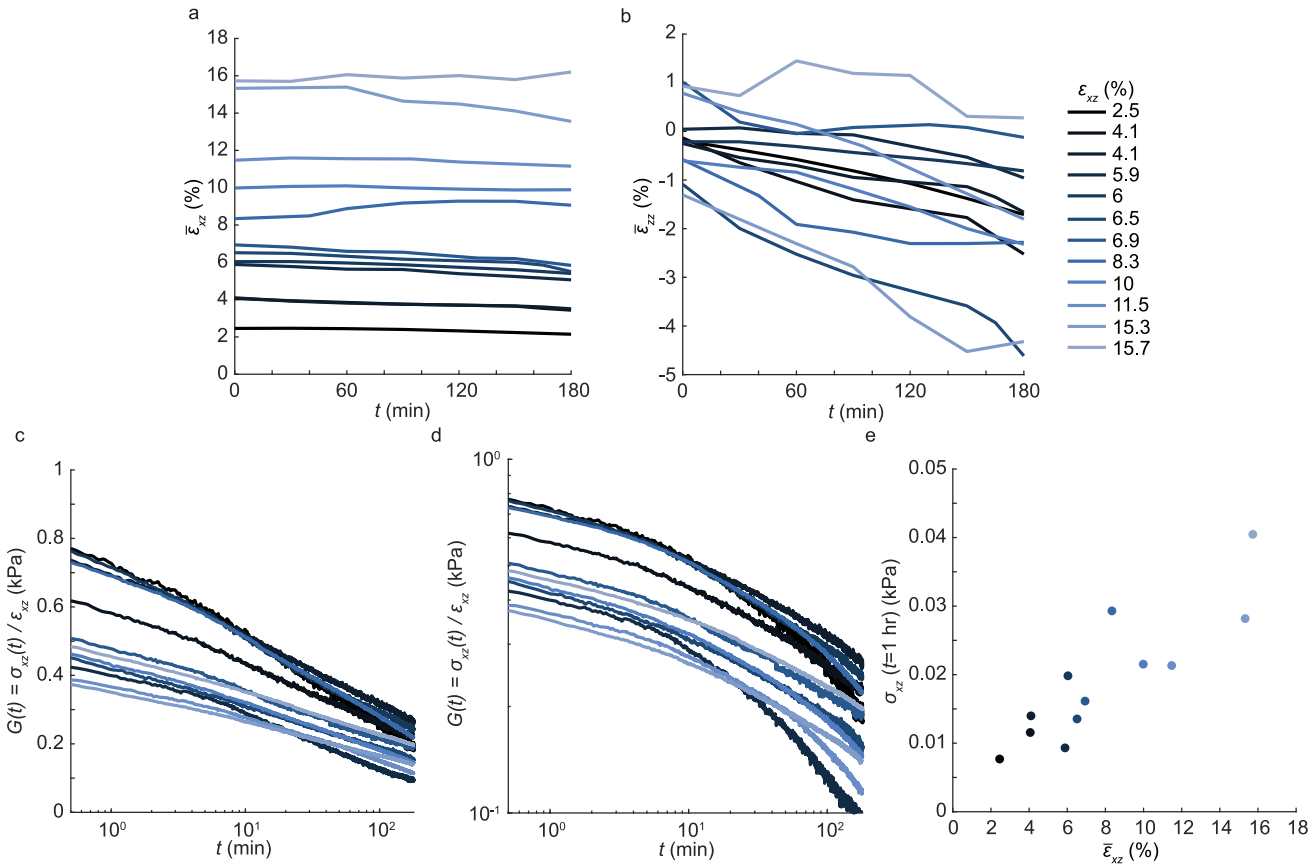


**Fig. 6** Shear stress relaxation on CNF gels. (**a**) Mean shear strains and (**b**) mean normal strains in the $z$-direction quantified from DIC. (**c, d**) Relaxation moduli of CNF gels at varying strains is presented on (c) semi-log and (d) log-log axes. Sample-to-sample variability caused $G(t)$ to vary by a factor of 2. (**e**) Shear stress in the gels at 1 hr against average shear strain at the same time point

to discern if recovery before the final loading would affect the variability in $G(t)$ (Fig. 7(c)). Even with a 1 hr wait time after pre-conditioning, the variability in $G(t)$ was still lower than $G(t)$ of CNF gels that did not undergo pre-conditioning (Fig. 7(a)). We note that while pre-conditioning can decrease variability between samples, the data presented in Fig. 6 may be more accurate for applications where pre-conditioning cannot be performed.

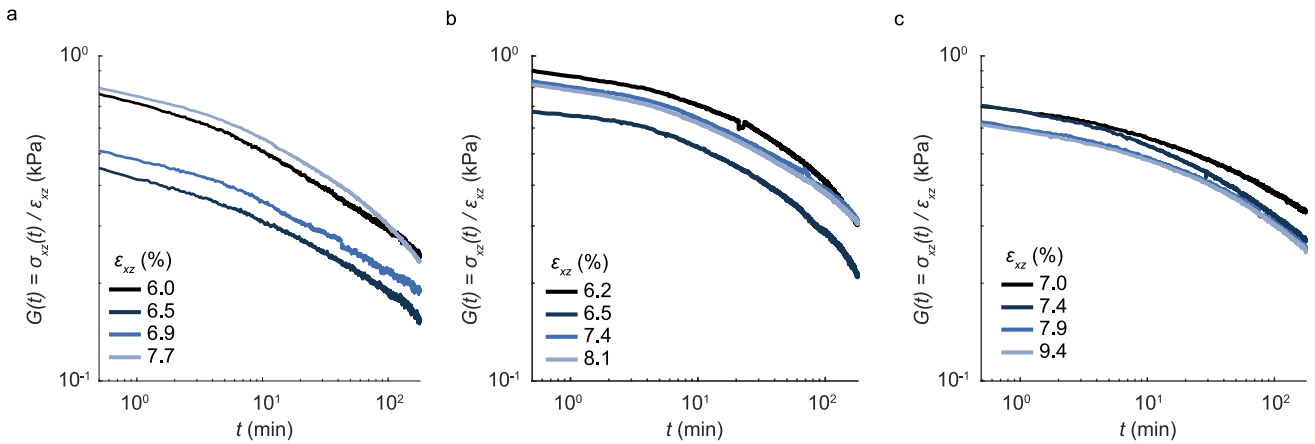


**Fig. 7** Effects of pre-conditioning on sheared CNF gels. (**a**) Relaxation moduli of CNF gels that did not undergo pre-conditioning. (**b**) Relaxation moduli of pre-conditioned CNF gels with no wait time between pre-conditioning and the stress relaxation experiment. (**c**) Relaxation moduli of pre-conditioned CNF gels with a 1 hr wait step between pre-conditioning and the stress relaxation experiment

## Fitting Relaxation Modulus to a Constitutive Model

The data of relaxation moduli $G(t)$ (shown in Figs. 5–7) were plotted on both semi-logarithmic and logarithmic axes. The curves of $G(t)$ were not straight lines on either set of axes, meaning $G(t)$ did not decay as a simple exponential or power law. To identify an effective constitutive model for fitting the data, we considered a modified form of the standard linear solid, with the viscous element replaced by a fractional derivative element [43]. The stress relaxation behavior of this model is given by

$$G(t) = A - B(t/\tau)^n$$

where $A$, $B$, $\tau$, and $n$ are fitting constants, with $n$ indicating the order of the fractional derivative. Only three of the four fitting constants are independent. To perform the fitting, we rewrote the equation as

$$\log(A - G(t)) = n\log(t) + (\log(B) - n\log(\tau))$$

We noted that $A = G(0)$. Given that one constant must be chosen arbitrarily, we defined $B = A/2$, in which case the constant $\tau$ will indicate the time for the CNF gel to relax to half of its initial modulus. The remaining two constants were then determined by a linear least-square error fit. Figure 8(a) shows a representative relaxation modulus data set plotted along with the fitted constitutive model. Fitted values for the three independent constants are shown in (Fig. 8(b–d)). The fitting constant $A = G(0)$ ranged from 0.4–1.1 kPa (Fig. 8(b)). The characteristic relaxation time $\tau$ for CNF gels that were not pre-conditioned increased with increasing shear strain, from ∼25 min to ∼45 min (Fig. 8(c)). This positive correlation was statistically significant, as confirmed by a Pearson's correlation test between shear strain and characteristic relaxation time ($R = 0.72$, $p = 0.008$). Interestingly, $\tau$ in CNF gels that were pre-conditioned was between 45–90 min, larger than in gels without pre-conditioning. This observation indicates that pre-conditioning may have caused some initial reconfiguration of the microstructure. The power $n$ did not show a notable change with increasing $\bar{\varepsilon}_{xz}$, and was in the range ≈0.20–0.35 (Fig. 8(d)), which indicates relaxation over many decades in time.

## Triaxial Compression and Compliance

The next experiment performed to quantify mechanics of CNF gels subjected them to triaxial compression. As described in the Methods section, thin samples were compressed between parallel plates, which produced compressive stresses in all directions. The experiment was load controlled, and the creep compliance $J(t)$ was quantified by dividing the engineering strain $\varepsilon_{zz}(t)$ by the applied stress $\sigma_{zz}$.

In Fig. 9, data are shown for a representative set of tests on a CNF gel of 1.99 wt%. Tests were performed at varying applied stress, ranging from ≈0.1 to 4.5 kPa. Interestingly, the data showed notable differences at low applied stress ($<$ 2 kPa) compared to high ($\geq$ 2 kPa). At low applied stress (Fig. 9(a)), the creep compliance increased over time. This increase on logarithmic axes was approximately linear for time points $t \geq 10$ min, denoting a power law relationship with a mean slope of approximately 1.2. Additionally, the creep compliance at long time decreased monotonically with applied stress, indicating nonlinear material behavior. At high magnitudes of applied stress (Fig. 9(b)), the behavior in time was different—the slopes of the curves were much flatter, indicating a smaller change in the creep compliance over time. Additionally, for stresses in the range of ≈3.5–4.5 kPa, the creep compliance was nearly constant over time. Hence, the CNF gels of 1.99 wt% exhibited different mechanical behaviors for compressive stress below and above 2 kPa. To plot the results for varying applied compressive stress together, the compressive strain of each CNF gel at the 1 hr time point was plotted against the compressive

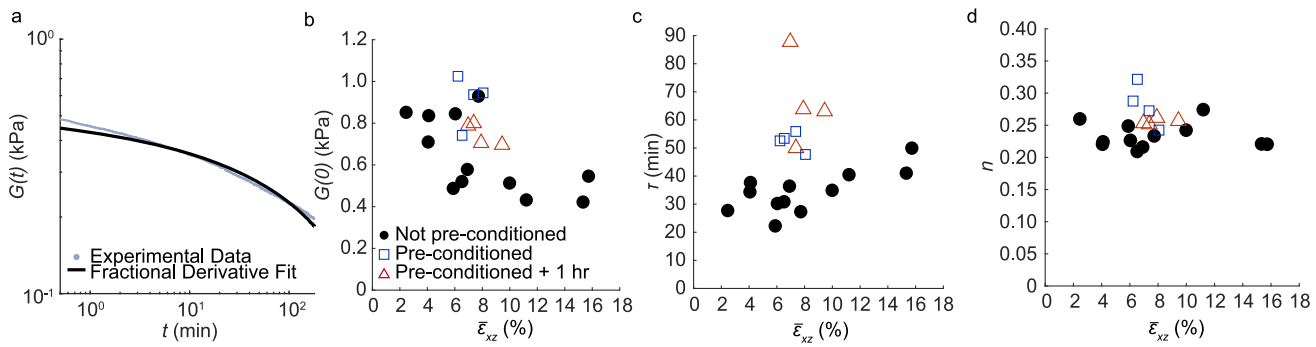


**Fig. 8** Fitting relaxation modulus to fractional derivative model. (**a**) Fractional derivative fit is plotted above experimental data of a shear relaxation modulus of a representative CNF gel. (**b**) Parameter $G(0)$, which indicates the relaxation modulus at short time. (**c**) Characteristic relaxation time $\tau$ increased from ≈25 min to ≈45 min with increasing shear strain in CNF gels that were not pre-conditioned. (**d**) Exponent for $(t/\tau)^n$ in all CNF gels tested was approximately 0.20–0.35 across all shear strains

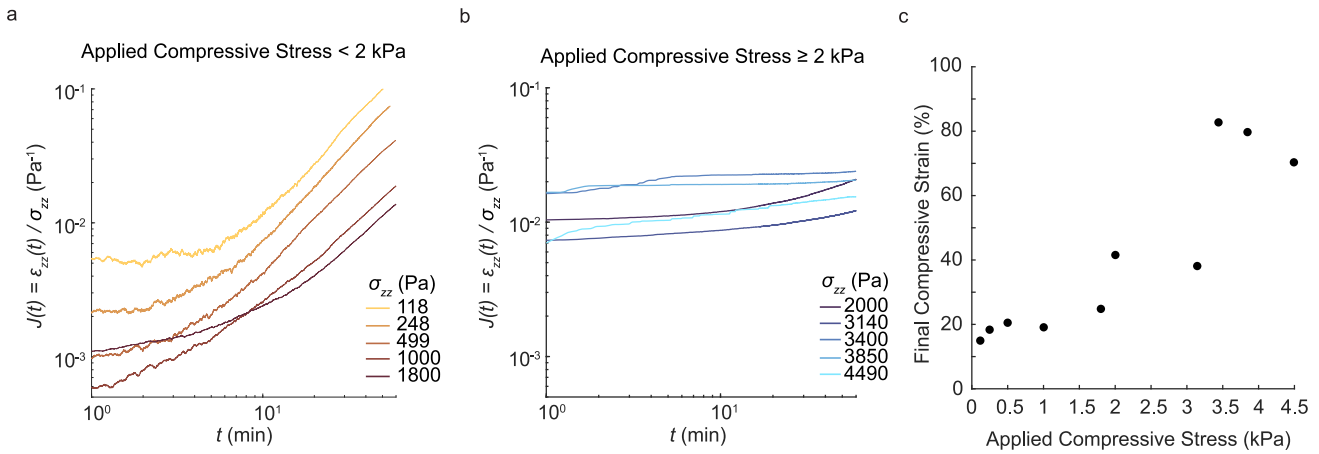


**Fig. 9** Response of CNF gels of 1.99 wt% to triaxial compression. (**a, b**) Compliance $J(t)$ of CNF gels of 1.99 wt% is plotted against time on logarithmic axes for applied compressive stress below 2 kPa (a) and above 2 kPa (b). At low applied stress (a), in the first 10 min the gel resisted deformation, shown by $J(t)$ fluctuating with no notable increase in magnitude. After around 10 min, the compliance increased over time. At long times, the compliance decreased with increasing stress. (b) At higher applied stresses, $J(t)$ plateaued quickly, and there was no notable increase or decrease as applied stress increased. (**c**) Final compressive strain versus applied compressive stress plotted on linear axes for CNF gels of 2 wt% concentration

stress (Fig. 9(c)). Although the resulting data was approximately linear, it was offset from the origin at small applied stress. The compliance $J(t)$ in (Fig. 9(a–b)) can be understood as a secant compliance, meaning that $J$ can be observed in (Fig. 9(c)) by taking the slope of a line drawn from the origin to a data point on the plot. Therefore, the offset from the origin at small stress creates a pronounced nonlinearity, which is most notable at smaller values of applied stress, as observed in (Fig. 9(a)).

The different mechanics above and below a critical stress can be explained by the fact that these boundary conditions change both the shape and the volume of the material. Given that the water in the CNF gels is incompressible, volume change requires the water to drain from the gel, which occurs readily after the gel's osmotic pressure is exceeded [36]. Similar observations have been made in other hydrogels, such as polyacrylamide [36–38]. To study the effect of osmotic pressure, we followed the procedure proposed by Ref. [36], which plotted the compressive strain against stress. Because the creep compliance data in our experiment depended on time, we chose to use the strain and stress at the 1 hr time point of each test. We performed experiments for five concentrations ranging from 0.95 to 5 wt% (Fig. 10(a)). Results of compressive strain against applied compressive stress at the 1 hr time point are reported in (Fig. 10(a)). Across all concentrations, two distinct regimes were present, consistent with the two distinct behaviors in compliance shown in (Fig. 9(a) and (b)). In the first regime, the slope of compres-

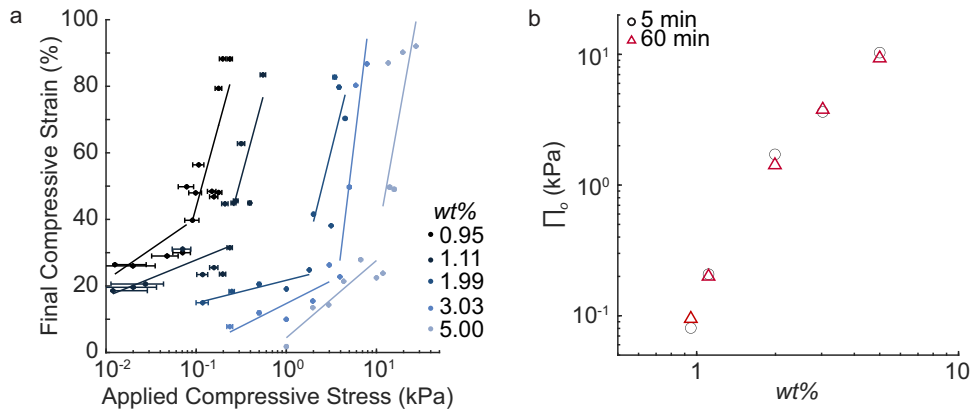


**Fig. 10** Quantifying osmotic pressure in CNF gels of various concentrations. (**a**) Compressive strain at the final time point (defined as the 1 hr time point of each experiment) is plotted against applied compressive stress on semi-log axes in CNF gels of five different weight percentages. Each point represents an independent sample. Error bars represent standard deviation over the final 5 min. The vertical error bars are sometimes smaller than the data points in the plot. (**b**) Measured osmotic pressure plotted against concentration on logarithmic axes for data acquired after 5 min and 1 hr of applied stress

sive strain against applied compressive stress was flatter than in the second regime, indicating less compliance (*i.e.*, greater stiffness) in the first regime compared to the second.

By visual inspection of the samples during these experiments, we observed that in the first regime, water did not flow out of the gels, whereas in the second regime it did. These qualitative observations support the idea that the transition between regimes is caused by exceeding a critical osmotic pressure. To gain further intuition for this behavior, we calculated the Poisson's ratio that an isotropic, linear, and elastic material would have under these boundary conditions. We note that it is unknown how isotropic the CNF gels tested here are, the CNF gels are viscoelastic rather than elastic, and deformations are finite, meaning that this calculation will give only a rough approximation for the apparent Poisson's ratio of CNF gels, but it is nevertheless informative as an indicator of how close to incompressible the CNF gels are in the two regimes. For the calculation, we used the data of strain against stress (Fig. 10(a)) and the data from Fig. 6 on the shear modulus at the same 1 hr time point. These data, plus the constitutive relationship for an isotropic, linear, elastic material allow for computing the approximate Poisson's ratio. In the first regime of strain response in (Fig. 10(a)), the approximate Poisson's ratio across all samples was $\approx 0.49$, nearly equal to the incompressible limit of 0.5. For the second regime, the approximate Poisson's ratio was $\approx 0.37$, indicating that in this regime the material was compressible, which is consistent with the explanation posed above, that water drains from the gel after the osmotic pressure is exceeded. To gain a sense of the stress state during this experiment, we computed $\nu/(1-\nu)$, which, as described in the Methods section, is equal to the ratio of the in-plane stresses to the applied normal stress for a isotropic, linear, elastic material. From the approximate Poisson's ratios stated above, the ratio is $\approx 0.96$ in the first regime, which is close to unity, indicating a nearly hydrostatic state of pressure. In the second regime, the ratio is $\approx 0.58$, which indicates the stress state is not hydrostatic but is nevertheless triaxial.

We next quantified the osmotic pressure by measuring the transition point between the two regimes. To this end, we used least squares fitting to fit lines to the data in each regime, and quantified the osmotic pressure as being equal to the magnitude of compressive stress at the intersection between the two lines [36]. This procedure was repeated for all sample concentrations, and the results are shown in (Fig. 10(b)). The results indicate that the osmotic pressure increased with increasing fibril concentration, which is similar to prior studies of other gels [36, 37]. Finally, recognizing that these data used the 1 hr time point, we repeated the analysis for a different time point to verify that the relationship between osmotic pressure and concentration does not depend substantially on time. We used a time point of $t = 5$ min, and computed osmotic pressure for each sample. The trends in the data at the 5 min time point were largely the same, indicating that the osmotic pressure does not depend on time, but does depend on concentration (Fig. 10(b)).

## Conclusions

We have described experimental approaches to quantify the time-dependent mechanics of CNF gels. Our methods were designed to address two major challenges in working with this material. First, the material undergoes shear thinning and strain localization, which causes results to depend on sample size. Secondly, most prior work has viewed the material as a fluid, which complicates understanding of elastic storage of energy and has focused primarily on the mechanics in response to changes in shape rather than volume. We also summarize additional complications in working with CNF gels, namely nonlinearity, elastocapillary behavior, evaporation, swelling in the presence of water, and dependence on osmotic pressure. The experimental methods described here address these numerous complications, and the data provide insight into time-dependent mechanical behavior in response to changes in both shape and volume. The results from shear stress relaxation experiments indicate a viscoelastic relaxation time scale on the order of tens of minutes and a reasonable fit to a fractional derivative model. The results from the volume changing experiments suggest that creep compliance changes on the order of hours and that the mechanics depend on osmotic pressure, with the compliance being substantially different below and above the osmotic pressure.

It will be interesting to build on this work by identifying how observations about the mechanics reported here relate to the microstructure of the CNF gels. There are multiple interesting potential directions. For example, in shear, the variability in the relaxation modulus of CNF gels that underwent pre-conditioning was lower than that of CNF gels that did not undergo pre-conditioning. It is possible that this observation resulted from fibrils aligning in the direction of shear during the pre-conditioning step. As another example, fibril aggregation may be the underlying cause of the spatial heterogeneity in strains observed in the experiments. Testing these ideas will require developing experimental approaches that visualize the microstructure during loading, which is yet another important future direction.

**Author Contributions** Conceptualization: Jacob Notbohm; Methodology: Samir Patel and Jacob Notbohm; Formal analysis and investigation: Samir Patel, John Considine, and Jacob Notbohm; Writing: Samir Patel, John Considine, and Jacob Notbohm; Funding acquisition: Jacob Notbohm; Resources: John Considine and Jacob Notbohm; Supervision: John Considine and Jacob Notbohm.

**Funding** This work was supported by the Department of Mechanical Engineering at the University of Wisconsin-Madison and by the

United States Endowment for Forestry and Communities grant number 22-CA-11111129-049. The United States Endowment for Forestry and Communities, Inc. is a not-for-profit corporation that collaborates with partners in the public and private sectors to advance systemic, transformative, and sustainable change for the health and vitality of the nation's working forests and forest-reliant communities.

**Availability of Data and Materials** Data reported in this manuscript are available from the corresponding author upon reasonable request. Digital image correlation software used in this study is available at https://github.com/jknotbohm/FIDIC.

## Declarations

**Ethical Approval** This study did not use human or animal subjects.

**Competing Interests** We declare no conflict of interest relevant to the content in this manuscript.



## References

1. Azeredo HM, Barud H, Farinas CS, Vasconcellos VM, Claro AM (2019) Bacterial cellulose as a raw material for food and food packaging applications. Front Sustainable Food Syst 3:7
2. Li M-C, Wu Q, Moon RJ, Hubbe MA, Bortner MJ (2021) Rheological aspects of cellulose nanomaterials: Governing factors and emerging applications. Adv Mater 33(21):2006052
3. Etale A, Onyianta AJ, Turner SR, Eichhorn SJ (2023) Cellulose: a review of water interactions, applications in composites, and water treatment. Chem Rev 123(5):2016–2048
4. Lou Y-R, Kanninen L, Kuisma T, Niklander J, Noon LA, Burks D, Urtti A, Yliperttula M (2014) The use of nanofibrillar cellulose hydrogel as a flexible three-dimensional model to culture human pluripotent stem cells. Stem Cells Dev 23(4):380–392
5. Kumar V, Bollström R, Yang A, Chen Q, Chen G, Salminen P, Bousfield D, Toivakka M (2014) Comparison of nano-and microfibrillated cellulose films. Cellulose 21:3443–3456
6. Lee K-Y, Tammelin T, Schulfter K, Kiiskinen H, Samela J, Bismarck A (2012) High performance cellulose nanocomposites: comparing the reinforcing ability of bacterial cellulose and nanofibrillated cellulose. ACS Appl Mater Interfaces 4(8):4078–4086
7. Zhou C, Wu Q (2011) A novel polyacrylamide nanocomposite hydrogel reinforced with natural chitosan nanofibers. Colloids Surf B 84(1):155–162
8. Liao J, Pham KA, Breedveld V (2020) Rheological characterization and modeling of cellulose nanocrystal and tempo-oxidized cellulose nanofibril suspensions. Cellulose 27(7):3741–3757
9. Saito T, Kimura S, Nishiyama Y, Isogai A (2007) Cellulose nanofibers prepared by tempo-mediated oxidation of native cellulose. Biomacromol 8(8):2485–2491
10. Facchine EG, Spontak RJ, Rojas OJ, Khan SA (2020) Shear-dependent structures of flocculated micro/nanofibrillated cellulose (MNFC) in aqueous suspensions. Biomacromol 21(9):3561–3570
11. Nechyporchuk O, Belgacem MN, Pignon F (2016) Current progress in rheology of cellulose nanofibril suspensions. Biomacromol 17(7):2311–2320
12. Fneich F, Ville J, Seantier B, Aubry T (2019) Structure and rheology of aqueous suspensions and hydrogels of cellulose nanofibrils: Effect of volume fraction and ionic strength. Carbohydr Polym 211:315–321
13. Song HY, Park SY, Kim S, Youn HJ, Hyun K (2022) Linear and nonlinear oscillatory rheology of chemically pretreated and non-pretreated cellulose nanofiber suspensions. Carbohydr Polym 275:118765
14. Martoïa F, Perge C, Dumont P, Orgéas L, Fardin M, Manneville S, Belgacem M (2015) Heterogeneous flow kinematics of cellulose nanofibril suspensions under shear. Soft Matter 11(24):4742–4755
15. Mendoza L, Batchelor W, Tabor RF, Garnier G (2018) Gelation mechanism of cellulose nanofibre gels: A colloids and interfacial perspective. J Colloid Interface Sci 509:39–46
16. Zhou L, He H, Li M-C, Song K, Cheng H, Wu Q (2016) Morphological influence of cellulose nanoparticles (cns) from cottonseed hulls on rheological properties of polyvinyl alcohol/cn suspensions. Carbohydr Polym 153:445–454
17. Naderi A, Lindström T (2015) Rheological measurements on nanofibrillated cellulose systems: a science in progress. In: Mondal MIH (ed) Cellulose and Cellulose Derivatives: Synthesis, Modification and Applications. Nova Science Publishers, Incorporated, Hauppauge, NY, pp 187–204
18. Naderi A (2017) Nanofibrillated cellulose: properties reinvestigated. Cellulose 24(5):1933–1945
19. Nazari B, Kumar V, Bousfield DW, Toivakka M (2016) Rheology of cellulose nanofibers suspensions: boundary driven flow. J Rheol 60(6):1151–1159
20. Quennouz N, Hashmi SM, Choi HS, Kim JW, Osuji CO (2016) Rheology of cellulose nanofibrils in the presence of surfactants. Soft Matter 12(1):157–164
21. Shin S, Hyun J (2021) Rheological properties of cellulose nanofiber hydrogel for high-fidelity 3d printing. Carbohydr Polym 263:117976
22. Li M-C, Wu Q, Lei T, Mei C, Xu X, Lee S, Gwon J (2020) Thermothickening drilling fluids containing bentonite and dual-functionalized cellulose nanocrystals. Energy Fuels 34(7):8206–8215
23. Janeček E-R, McKee JR, Tan CS, Nykänen A, Kettunen M, Laine J, Ikkala O, Scherman OA (2015) Hybrid supramolecular and colloidal hydrogels that bridge multiple length scales. Angew Chem Int Ed 54(18):5383–5388
24. Mendoza DJ, Ayurini M, Browne C, Raghuwanshi VS, Simon GP, Hooper JF, Garnier G (2022) Thermoresponsive poly (n-isopropylacrylamide) grafted from cellulose nanofibers via silver-promoted decarboxylative radical polymerization. Biomacromol 23(4):1610–1621
25. Mohan S, Koenderink GH, Velikov KP (2018) Inelastic behaviour of cellulose microfibril networks. Soft Matter 14(33):6828–6834
26. Žepič V, Oven P, Čop M, Vek V, Janković B, Poljanšek I (2022) Physical, rheological and mechanical properties of alkali activated hydrogels based on nanofibrillated cellulose. J Nat Fibers 19(17):16040–16052
27. Torres FG, Troncoso OP, Lopez D, Grande C, Gomez CM (2009) Reversible stress softening and stress recovery of cellulose networks. Soft Matter 5(21):4185–4190

28. Nechyporchuk O, Belgacem MN, Pignon F (2014) Rheological properties of micro-/nanofibrillated cellulose suspensions: wall-slip and shear banding phenomena. Carbohydr Polym 112:432–439
29. Mohtaschemi M, Dimic-Misic K, Puisto A, Korhonen M, Maloney T, Paltakari J, Alava MJ (2014) Rheological characterization of fibrillated cellulose suspensions via bucket vane viscometer. Cellulose 21(3):1305–1312
30. Song J, Caggioni M, Squires TM, Gilchrist JF, Prescott SW, Spicer PT (2019) Heterogeneity, suspension, and yielding in sparse microfibrous cellulose gels 1. bubble rheometer studies. Rheol Acta 58(5):217–229
31. Saito T, Kimura S, Nishiyama Y, Isogai A (2007) Cellulose nanofibers prepared by TEMPO-mediated oxidation of native cellulose. Biomacromol 8(8):2485–2491. https://doi.org/10.1021/bm0703970
32. Heise K, Kontturi E, Allahverdiyeva Y, Tammelin T, Linder MB, Nonappa Ikkala O (2021) Nanocellulose: recent fundamental advances and emerging biological and biomimicking applications. Adv Mater 33(3):2004349
33. Yang X, Biswas SK, Han J, Tanpichai S, Li M-C, Chen C, Zhu S, Das AK, Yano H (2021) Surface and interface engineering for nanocellulosic advanced materials. Adv Mater 33(28):2002264
34. Bar-Kochba E, Toyjanova J, Andrews E, Kim K-S, Franck C (2015) A fast iterative digital volume correlation algorithm for large deformations. Exp Mech 55:261–274
35. Farid H, Simoncelli EP (2004) Differentiation of discrete multidimensional signals. IEEE Trans Image Process 13(4):496–508
36. Schulze KD, Hart SM, Marshall SL, O'Bryan CS, Urueña JM, Pitenis AA, Sawyer WG, Angelini TE (2017) Polymer osmotic pressure in hydrogel contact mechanics. Biotribology 11:3–7
37. Bhattacharyya A, O'Bryan C, Ni Y, Morley CD, Taylor CR, Angelini TE (2020) Hydrogel compression and polymer osmotic pressure. Biotribology 22:100125
38. O'Bryan CS, Ni Y, Taylor CR, Angelini TE, Schulze KD (2024) Collagen networks under indentation and compression behave like cellular solids. Langmuir 40(8):4228–4235
39. Poynting JH (1909) On pressure perpendicular to the shear planes in finite pure shears, and on the lengthening of loaded wires when twisted. Proc R Soc Lond A 82(557):546–559
40. Sharma A, Licup A, Jansen K, Rens R, Sheinman M, Koenderink G, MacKintosh F (2016) Strain-controlled criticality governs the nonlinear mechanics of fibre networks. Nat Phys 12(6):584–587
41. Storm C, Pastore JJ, MacKintosh FC, Lubensky TC, Janmey PA (2005) Nonlinear elasticity in biological gels. Nature 435(7039):191–194
42. Licup AJ, Münster S, Sharma A, Sheinman M, Jawerth LM, Fabry B, Weitz DA, MacKintosh FC (2015) Stress controls the mechanics of collagen networks. PNAS 112(31):9573–9578
43. Koeller R (1984) Applications of fractional calculus to the theory of viscoelasticity. J Appl Mech 51:299–307